Biogeosciences, 14, 1333–1348, 2017
www.biogeosciences.net/14/1333/2017/
doi:10.5194/bg-14-1333-2017

Biogeosciences Open Access EGU

Modelling spatial and temporal dynamics of gross primary production in the Sahel from earth-observation-based photosynthetic capacity and quantum efficiency

Torbern Tagesson[1,2], Jonas Ardö[2], Bernard Cappelaere[3], Laurent Kergoat[4], Abdulhakim Abdi[2], Stéphanie Horion[1], and Rasmus Fensholt[1]

[1]Department of Geosciences and Natural Resource Management, University of Copenhagen, Øster Voldgade 10, Ø 1350 Copenhagen, Denmark
[2]Department of Physical Geography and Ecosystem Science, Lund University, Sölvegatan 12, 223 62 Lund, Sweden
[3]HydroSciences Montpellier, IRD, CNRS, Univ. Montpellier, Montpellier, France
[4]Géosciences Environnement Toulouse, (CNRS/UPS/IRD), 14 av E Belin, 31400 Toulouse, France

Correspondence to: Torbern Tagesson (torbern.tagesson@ign.ku.dk)

Received: 27 September 2016 – Discussion started: 29 September 2016
Revised: 13 February 2017 – Accepted: 28 February 2017 – Published: 17 March 2017

Abstract. It has been shown that vegetation growth in semi-arid regions is important to the global terrestrial CO_2 sink, which indicates the strong need for improved understanding and spatially explicit estimates of CO_2 uptake (gross primary production; GPP) in semi-arid ecosystems. This study has three aims: (1) to evaluate the MOD17A2H GPP (collection 6) product against GPP based on eddy covariance (EC) for six sites across the Sahel; (2) to characterize relationships between spatial and temporal variability in EC-based photosynthetic capacity (F_{opt}) and quantum efficiency (α) and vegetation indices based on earth observation (EO) (normalized difference vegetation index (NDVI), renormalized difference vegetation index (RDVI), enhanced vegetation index (EVI) and shortwave infrared water stress index (SIWSI)); and (3) to study the applicability of EO upscaled F_{opt} and α for GPP modelling purposes. MOD17A2H GPP (collection 6) drastically underestimated GPP, most likely because maximum light use efficiency is set too low for semi-arid ecosystems in the MODIS algorithm. Intra-annual dynamics in F_{opt} were closely related to SIWSI being sensitive to equivalent water thickness, whereas α was closely related to RDVI being affected by chlorophyll abundance. Spatial and inter-annual dynamics in F_{opt} and α were closely coupled to NDVI and RDVI, respectively. Modelled GPP based on F_{opt} and α upscaled using EO-based indices reproduced in situ GPP well for all except a cropped site that was strongly impacted by anthropogenic land use. Upscaled GPP for the Sahel 2001–2014 was 736 ± 39 g C m^{-2} yr^{-1}. This study indicates the strong applicability of EO as a tool for spatially explicit estimates of GPP, F_{opt} and α; incorporating EO-based F_{opt} and α in dynamic global vegetation models could improve estimates of vegetation production and simulations of ecosystem processes and hydro-biochemical cycles.

1 Introduction

Vegetation growth in semi-arid regions is an important sink for fossil fuel emissions. Mean carbon dioxide (CO_2) uptake by terrestrial ecosystems is dominated by highly productive lands, mainly tropical forests, whereas semi-arid regions are the main biome driving its inter-annual variability (Ahlström et al., 2015; Poulter et al., 2014). Semi-arid regions contribute to 60 % of the long-term trend in the global terrestrial C sink (Ahlström et al., 2015). It is thus important to understand long-term variability of vegetation growth in semi-arid areas and the response of vegetation to environmental conditions to better quantify and forecast effects of climate change.

The Sahel is a semi-arid transition zone between the dry Sahara desert in the north and the humid Sudanian savanna in the south. The region has experienced numerous severe

droughts over the last decades, which resulted in region-wide famines in 1972–1973 and 1984–1985 and localized food shortages across the region in 1990, 2002, 2004, 2011 and 2012 (Abdi et al., 2014; United Nations, 2013). Vegetation production is thereby an important ecosystem service for livelihoods in the Sahel, but it is under threat. The region is experiencing strong population growth, increasing the demand on ecosystem services due to cropland expansion, increased pasture stocking rates and fuelwood extraction (Abdi et al., 2014).

At the same time as we have reports of declining vegetation production, we have contradicting reports of the greening of the Sahel based on earth observation (EO) data (Dardel et al., 2014; Fensholt et al., 2013). The greening of the Sahel has mainly been attributed to alleviated drought stress conditions due to increased precipitation since the mid-1990s (Hickler et al., 2005). Climate is thus another important factor regulating vegetation production. Semi-arid regions, such as the Sahel, are particularly vulnerable to climate fluctuations due to their dependency on moisture.

Estimation of gross primary production (GPP), i.e. uptake of atmospheric CO_2 by vegetation, is still a major challenge for the remote sensing of ecosystem services. Gross primary production is a main driver of ecosystem services such as climate regulation, carbon (C) sequestration, C storage, food production and livestock grassland production. Within EO, spatial quantification of GPP generally involves light use efficiency (LUE), defined as the conversion efficiency of absorbed solar light into CO_2 uptake (Monteith, 1972, 1977). It has been shown that LUE varies in space and time due to factors such as plant functional type, drought and temperature, nutrient levels, and physiological limitations of photosynthesis (Garbulsky et al., 2010; Paruelo et al., 2004; Kergoat et al., 2008). The LUE concept has been applied through various methods, either by using a biome-specific LUE constant (Ruimy et al., 1994) or by modifying a maximum LUE using meteorological variables (Running et al., 2004).

An example of a LUE-based model is the standard GPP product from the Moderate Resolution Imaging Spectroradiometer (MODIS) sensor (MOD17A2). Within the model, absorbed photosynthetically active radiation (PAR) is estimated as a product of the fraction of PAR absorbed by green vegetation (FPAR from MOD15A2) multiplied with daily PAR from the meteorological data of the Global Modeling and Assimilation Office (GMAO). A set of maximum LUE parameters specified for each biome are extracted from a Biome Properties Look-Up Table (BPLUT). Then maximum LUE is modified depending on air temperature (T_{air}) and vapour pressure deficit (VPD; Running et al., 2004). Sjöström et al. (2013) evaluated the MOD17A2 product (collection 5.1) for Africa and showed that it underestimated GPP for semi-arid savannas in the Sahel. Explanations for this underestimation were that the assigned maximum LUE from BPLUT was set too low and that there were uncertainties in the FPAR product (MOD15A2). Recently, a new collection of MOD17A2 at a 500 m spatial resolution was released (MOD17A2H, collection 6) with an updated BPLUT, updated GMAO meteorological data, improved quality control and gap-filling of the FPAR data from MOD15A2 (Running and Zhao, 2015).

It has been shown that the LUE method does not perform well in arid conditions and at agricultural sites (Turner et al., 2005). Additionally, the linearity assumed by the LUE model is not usually found as the response of GPP to incoming light follows more of an asymptotic curve (Cannell and Thornley, 1998). Investigating other methods for remotely determining GPP is thus of great importance, especially for semi-arid environments. Therefore, instead of LUE, we focus on the light response function of GPP at the canopy scale, and spatial and temporal variation of its two main parameters: maximum GPP under light saturation (canopy-scale photosynthetic capacity, F_{opt}) and the initial slope of the light response function (canopy-scale quantum efficiency, α; Falge et al., 2001; Tagesson et al., 2015a). Photosynthetic capacity is a measure of the maximum rate at which the canopy can fix CO_2 during photosynthesis ($\mu mol\, CO_2\, m^{-2}\, s^{-1}$), whereas α is the amount of CO_2 fixed per incoming PAR ($\mu mol\, CO_2\, \mu mol\, PAR^{-1}$). To clarify the difference in LUE and α in this study, LUE ($\mu mol\, CO_2\, \mu mol\, APAR^{-1}$) is the slope of a linear fit between CO_2 uptake and absorbed PAR, whereas α ($\mu mol\, CO_2\, \mu mol\, PAR^{-1}$) is the initial slope of an asymptotic curve against incoming PAR.

It has been proven that F_{opt} and α are closely related to chlorophyll abundance due to their coupling with the electron transport rate (Ide et al., 2010). Additionally, in semi-arid ecosystems, water availability is generally considered to be the main limiting factor affecting intra-annual dynamics of vegetation growth (Fensholt et al., 2013; Hickler et al., 2005; Tagesson et al., 2015b). Several remote sensing studies have established relationships between remotely sensed vegetation indices and ecosystem properties such as chlorophyll abundance and equivalent water thickness (Yoder and Pettigrew-Crosby, 1995; Fensholt and Sandholt, 2003). In this study, we will analyse whether EO vegetation indices can be used to upscale F_{opt} and α and investigate whether this could offer a promising way to map GPP in semi-arid areas. This potential will be analysed by the use of detailed ground observations from six eddy covariance (EC) flux tower sites across the Sahel.

The three aims of this study are

1. to investigate whether the recently released MOD17A2H GPP (collection 6) product is better at capturing GPP for the Sahel than collection 5.1. We hypothesize that the MOD17A2H GPP (collection 6) product will estimate GPP well for the six Sahelian EC sites because of major changes made in comparison to collection 5.1 (Running and Zhao, 2015);

2. to characterize the relationships between spatial and temporal variability in F_{opt} and α and remotely sensed

vegetation indices. We hypothesise that EO vegetation indices that are closely related to chlorophyll abundance will be most strongly coupled with spatial and inter-annual dynamics in F_{opt} and α, whereas vegetation indices closely related to equivalent water thickness will be most strongly coupled with intra-annual dynamics in F_{opt} and α across the Sahel;

3. to evaluate the applicability of a GPP model based on the light response function using EO vegetation indices and incoming PAR as input data.

2 Materials and methods

2.1 Site description

The Sahel stretches from the Atlantic Ocean in the west to the Red Sea in the east. The northern border towards the Sahara and the southern border towards the humid Sudanian savanna are defined by the 150 and 700 mm isohyets, respectively (Fig. 1; Prince et al., 1995). Tree and shrub canopy cover is now generally low (< 5 %) and dominated by species of *Balanites*, *Acacia, Boscia* and *Combretaceae* (Rietkerk et al., 1996). Annual grasses such as *Schoenefeldia gracilis*, *Dactyloctenium aegyptium*, *Aristida mutabilis* and *Cenchrus biflorus* dominate the herbaceous layer, but perennial grasses such as *Andropogon gayanus* and *Cymbopogon schoenanthus* can also be found (Rietkerk et al., 1996; de Ridder et al., 1982). From the FLUXNET database (Baldocchi et al., 2001) we selected six measurement sites with EC-based CO_2 flux data from the Sahel (Table 1; Fig. 1). The sites represent a variety of ecosystems present in the region, from dry fallow bush savanna to seasonally inundated acacia forest. For a full description of the measurement sites, we refer to Tagesson et al. (2016a) and references in Table 1.

2.2 Data collection

2.2.1 Eddy covariance and hydrometeorological in situ data

Eddy covariance and hydrometeorological data originating from the years between 2005 and 2013 were collected from the principal investigators of the measurement sites (Tagesson et al., 2016a). The EC sensor set-up consisted of open-path CO_2 and H_2O infrared gas analysers and three-axis sonic anemometers. Data were collected at 20 Hz and statistics were calculated for 30 min periods. For a full description of the sensor set-up and post processing of EC data, see the references in Table 1. Final fluxes were filtered according to quality flags provided by FLUXNET and outliers were filtered according to Papale et al. (2006). We extracted the original net ecosystem exchange (NEE) data without any gap-filling or partitioning of NEE to GPP and ecosystem respiration. The hydrometeorological data collected were air temperature (T_{air}, °C), rainfall (P, mm), relative air humidity (Rh, %), soil moisture at 0.1 m depth (SWC, % volumetric water content), incoming global radiation (R_g, $W\,m^{-2}$), incoming photosynthetically active radiation (PAR, $\mu mol\,m^{-2}\,s^{-1}$), VPD (hPa), peak dry weight biomass (g dry weight m^{-2}), C3 / C4 species ratio and soil conditions (nitrogen and C concentration, %). For a full description of the collected data and sensor set-up, see Tagesson et al. (2016a).

2.2.2 Earth observation data and gridded ancillary data

Composite products from MODIS/Terra covering the Sahel were acquired at Reverb ECHO (NASA, 2016). Collected products were GPP (MOD17A2H, collection 6), nadir bidirectional reflectance distribution function adjusted reflectance (NBAR; 8-day composites; MCD43A4, collection 5.1) at $500 \times 500\,m^2$ spatial resolution, the normalized difference vegetation index (NDVI) and the enhanced vegetation index (EVI; 16-day composites; MOD13Q1; collection 6) at $250 \times 250\,m^2$ spatial resolution. The NBAR product was preferred over the reflectance product (MOD09A1) in order to avoid variability caused by varying sun and sensor viewing geometry (Huber et al., 2014; Tagesson et al., 2015c). We extracted the median of 3×3 pixels centred at the location of each EC tower. Time series of EO products were filtered according to MODIS quality control data. MOD17A2H is a gap-filled and filtered product, and QC data from MCD43A2 were used for filtering of MCD43A4. Bit 2–5 (highest-decreasing quality) was used for MOD13Q1. Finally, data were gap-filled to daily values using linear interpolation.

We downloaded ERA Interim reanalysis PAR at the ground surface ($W\,m^{-2}$) with a spatial resolution of $0.25° \times 0.25°$ accumulated for each 3 h period from 2000 to 2014 from the European Centre for Medium-Range Weather Forecasts (ECMWF) (Dee et al., 2011; ECMWF, 2016a).

2.3 Data handling

2.3.1 Intra-annual dynamics in photosynthetic capacity and quantum efficiency

To estimate daily values of EC-based F_{opt} and α, the asymptotic Mitscherlich light-response function was fitted between daytime NEE and incoming PAR using a 7-day moving window with a 1-day time step:

$$NEE = -(F_{opt}) \times (1 - e^{\left(\frac{-\alpha \times PAR}{F_{opt}}\right)}) + R_d, \quad (1)$$

where F_{opt} is CO_2 uptake at light saturation (photosynthetic capacity; $\mu mol\,CO_2\,m^{-2}\,s^{-1}$), R_d is dark respiration ($\mu mol\,CO_2\,m^{-2}\,s^{-1}$) and α is the initial slope of the light response curve (quantum efficiency; $\mu mol\ CO_2\,\mu mol\ PAR^{-1}$;

Table 1. Description of the six measurement sites, including location, soil type, ecosystem type and dominant species.

Measurement site	Coordinates	Soil type	Ecosystem	Dominant species
Agoufou[a] (ML-AgG, Mali)	15.34° N, 1.48° W	Sandy ferruginous Arenosol	Open woody savanna (4 % tree cover)	Trees: *Acacia* spp., *Balanites aegyptiaca*, *Combretum glutinosum* Herbs: *Zornia glochidiata* *Cenchrus biflorus, Aristida mutabilis, Tragus berteronianus*
Dahra[b] (SN-Dah, Senegal)	15.40° N, 15.43° W	Sandy luvic Arenosol	Grassland and/or shrubland Savanna (3 % tree cover)	Trees: *Acacia* spp., *Balanites aegyptiaca* Herbs: *Zornia latifolia*, *Aristida adscensionis*, *Cenchrus biflorus*
Demokeya[c] (SD-Dem, Sudan)	13.28° N, 30.48° E	Cambic Arenosol	Sparse acacia savannah (7 % tree cover)	Trees: *Acacia* spp., Herbs: *Aristida pallida*, *Eragrostis tremula*, *Cenchrus biflorus*
Kelma[a] (ML-Kem, Mali)	15.22° N, 1.57° W	Clay soil depression	Open acacia forest (90 % tree cover)	Trees: *Acacia seyal*, *Acacia nilotica, Balanites aegyptiaca*, Herbs: *Sporobolus hevolvus* *Echinochloa colona*, *Aeschynomene sensitive*
Wankama Fallow[d] (NE-WaF, Niger)	13.65° N, 2.63° E	Sandy ferruginous Arenosol	Fallow bush	*Guiera senegalensis*
Wankama Millet[e] (NE-WaM, Niger)	13.64° N, 2.63° E	Sandy ferruginous Arenosol	Millet crop	*Pennisetum glaucum*

[a] Timouk et al. (2009). [b] Tagesson et al. (2015b). [c] Sjöström et al. (2009). [d] Velluet et al. (2014). [e] Boulain et al. (2009).

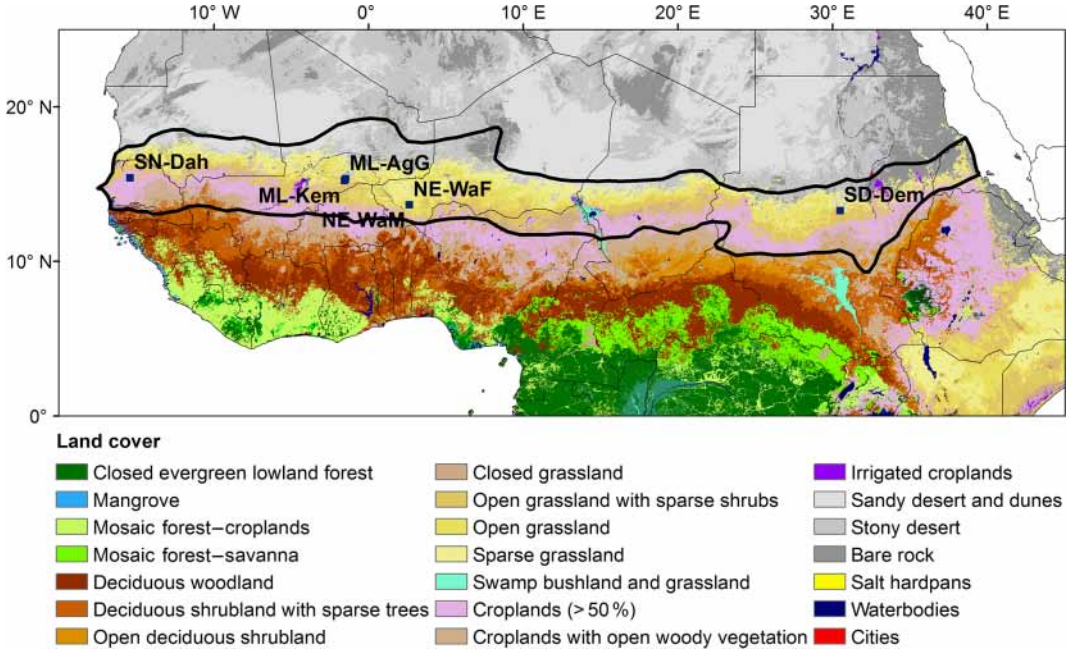

Figure 1. Land cover classes for the Sahel and the location of the six measurement sites of this study. The land cover classes are based on multi-sensor satellite observations (Mayaux et al., 2003). The sites are Agoufou (ML-AgG), Dahra (SN-Dah), Demokeya (SD-Dem), Kelma (ML-Kem), Wankama Fallow (NE-WaF) and Wankama Millet (NE-WaM). The thick black line delineates borders of the Sahel based on annual 150 and 700 mm isohyets (Prince et al., 1995).

Falge et al., 2001). By subtracting R_d from Eq. (1), the function was forced through zero and GPP was thereby estimated. To ensure a high quality of fitted parameters, parameters were excluded from the analysis when fitting was insignificant (p value > 0.05) and when they were out of range (F_{opt} and α > peak value of the rainy season times 1.2). Additionally, outliers were filtered following the method by Papale et al. (2006) using a 30-day moving window with a 1-day time step.

2.3.2 Vegetation indices

The maximum absorption in red wavelengths generally occurs at 682 nm as this is the peak absorption for chlorophyll *a* and *b* (Thenkabail et al., 2000), which makes vegetation indices that include the red band sensitive to chlorophyll abundance. By far the most common vegetation index is NDVI (Rouse et al., 1974):

$$\mathrm{NDVI} = \frac{(\rho_{\mathrm{NIR}} - \rho_{\mathrm{red}})}{(\rho_{\mathrm{NIR}} + \rho_{\mathrm{red}})}, \quad (2)$$

where ρ_{NIR} is the reflectance factor in the near-infrared (NIR) band (band 2) and ρ_{red} is the reflectance factor in the red band (band 1). Near-infrared radiance is reflected by leaf cells since absorption of these wavelengths would result in overheating of the plant, whereas red radiance is absorbed by chlorophyll and its accessory pigments (Gates et al., 1965). Normalization is done to reduce effects of atmospheric errors, solar zenith angles and sensor viewing geometry, as well as to increase the vegetation signal (Qi et al., 1994; Inoue et al., 2008).

A well-known deficiency of NDVI is problems of index saturation at high biomass because absorption of red light at $\sim$ 670 nm peaks at higher biomass loads, whereas NIR reflectance continues to increase due to multiple scattering effects (Mutanga and Skidmore, 2004; Jin and Eklundh, 2014). By reducing atmospheric and soil background influences, EVI is designed to increase the signal from the vegetation and maintain sensitivity in high biomass regions (Huete et al., 2002).

$$\mathrm{EVI} = G\frac{(\rho_{\mathrm{NIR}} - \rho_{\mathrm{red}})}{(\rho_{\mathrm{NIR}} + C_1\rho_{\mathrm{red}} - C_2\rho_{\mathrm{blue}} + L)}, \quad (3)$$

where ρ_{blue} is the reflectance factor in the blue band (band 3). The coefficients $C_1 = 6$ and $C_2 = 7.5$ correct for atmospheric influences, while $L = 1$ adjusts for the canopy background. The factor $G = 2.5$ is a gain factor.

Another attempt to overcome problems of NDVI saturation was proposed by Roujean and Breon (1995), who suggested the renormalized difference vegetation index (RDVI), which combines advantages of DVI (NIR-red) and NDVI for low and high vegetation cover, respectively:

$$\mathrm{RDVI} = \frac{(\rho_{\mathrm{NIR}} - \rho_{\mathrm{red}})}{\sqrt{(\rho_{\mathrm{NIR}} + \rho_{\mathrm{red}})}}. \quad (4)$$

As a non-linear index, RDVI is not only less sensitive to variations in geometrical and optical properties of unknown foliage but also less affected by solar and viewing geometry (Broge and Leblanc, 2001).

The NIR and shortwave infrared (SWIR) bands are affected by the same ground properties, except that SWIR bands are also strongly sensitive to equivalent water thickness. Fensholt and Sandholt (2003) proposed a vegetation index, the shortwave infrared water stress index (SIWSI), using NIR and SWIR bands to estimate drought stress for vegetation in semi-arid environments:

$$\mathrm{SIWSI}_{12} = \frac{(\rho_{\mathrm{NIR}} - \rho_{\mathrm{SWIR12}})}{(\rho_{\mathrm{NIR}} + \rho_{\mathrm{SWIR12}})} \quad (5)$$

$$\mathrm{SIWSI}_{16} = \frac{(\rho_{\mathrm{NIR}} - \rho_{\mathrm{SWIR16}})}{(\rho_{\mathrm{NIR}} + \rho_{\mathrm{SWIR16}})}, \quad (6)$$

where ρ_{SWIR12} is NBAR band 5 (1230–1250 nm) and ρ_{SWIR16} is NBAR band 6 (1628–1652 nm). As the vegetation water content increases, reflectance in SWIR decreases, indicating that low and high SIWSI values point to sufficient water conditions and drought stress, respectively. The vegetation indices RDVI, SIWSI_{12} and SIWSI_{16} were calculated based on NBAR bands 1, 2, 5 and 6.

2.3.3 Incoming PAR across the Sahel

A modified version of the ERA Interim reanalysis PAR was used in the current study as there was an error in the code producing these PAR estimates; the estimates were generally too low (ECMWF, 2016b). Accordingly, incoming PAR at the ground surface from ERA Interim was systematically underestimated even though it followed the pattern of PAR measured at the six Sahelian EC sites (Fig. S1 in Supplement). In order to correct for this error, we fitted and applied an ordinary least squares linear regression between in situ PAR and ERA Interim PAR (Fig. S1). The PAR produced from this relationship is at the same level as in situ PAR and should be at a correct level even though the original ERA Interim PAR is actually produced from the red and near-infrared part of the spectrum.

2.4 Data analysis

2.4.1 Coupling temporal and spatial dynamics in photosynthetic capacity and quantum efficiency with explanatory variables

The coupling between intra-annual dynamics in F_{opt} and α and the vegetation indices for the different measurement sites were studied using Pearson correlation analysis. As part of the correlation analysis, we used a bootstrap simulation methodology with 200 iterations from which the mean and the standard deviation (SD) of the correlation coefficients were calculated (Richter et al., 2012). Relationships between intra-annual dynamics in F_{opt} and α and the vegetation in-

dices for all sites combined were also analysed. In the analysis for all sites, data were normalized to avoid influence of spatial and inter-annual variability. Time series of ratios of F_{opt} and α (F_{opt_frac} and α_{frac}) against the annual peak values (F_{opt_peak} and α_{peak}; see below for calculation of annual peak values) were estimated for all sites:

$$F_{opt\_frac} = \frac{F_{opt}}{F_{opt\_peak}} \quad (7)$$

$$\alpha_{frac} = \frac{\alpha}{\alpha_{peak}}. \quad (8)$$

The same standardization procedure was used for all vegetation indices (VI_{frac}):

$$VI_{frac} = \frac{VI}{VI_{peak}}, \quad (9)$$

where VI_{peak} is the annual peak values of the vegetation indices (14-day running mean with highest annual value). The α_{frac} and F_{opt_frac} were correlated with the different VI_{frac} to investigate the coupling between intra-annual dynamics in F_{opt} and α and the vegetation indices for all sites.

Regression trees were used to fill gaps in the daily estimates of F_{opt} and α. Based on 100 cross-validation runs, 100 tree sizes were chosen, and these trees were then used to estimate F_{opt} and α following the method in De'ath and Fabricius (2000). We used SWC, VPD, T_{air}, PAR and the vegetation index with the strongest correlation with intra-annual dynamics as explanatory variables in the analysis. In the analysis for all sites, the same standardization procedure as done for F_{opt}, α and the vegetation indices was done for the hydrometeorological variables. The 100 F_{opt} and α output subsets from the regression trees were averaged and used for filling gaps in the times series of F_{opt} and α. From these time series, we estimated annual peak values of F_{opt} and α (F_{opt_peak} and α_{peak}) as the 14-day running mean with the highest annual value. To investigate spatial and inter-annual variability in F_{opt} and α across the measurement sites of the Sahel, F_{opt_peak} and α_{peak} were correlated with the annual sum of P; yearly means of T_{air}, SWC, RH, VPD and R_g; annual peak values of biomass; soil nitrogen and C concentrations; the C3 / C4 ratio; and VI_{peak}.

2.4.2 Parameterization and evaluation of the GPP model and evaluation of the MODIS GPP

On the basis of Eq. (1) and the outcome of the statistical analysis previously described under Sect. 2.4.1 (for results, see Sect. 3.2), a model for estimating GPP across the Sahel was created:

$$GPP = -F_{opt} \times \left(1 - e^{\left(\frac{-\alpha \times PAR}{F_{opt}}\right)}\right). \quad (10)$$

Firstly, F_{opt_peak} and α_{peak} were estimated spatially and inter-annually using linear regression functions fitted against the vegetation indices, with the strongest relationships to spatial and inter-annual variability in F_{opt_peak} and α_{peak} for all sites. Secondly, exponential regression functions were established for F_{opt_frac} and α_{frac} with the vegetation index, with the strongest relationships with intra-annual variability of F_{opt_frac} and α_{frac} for all sites. By combining these relationships, F_{opt} and α can be calculated for any day of year and for any point in space across the Sahel:

$$\begin{aligned} F_{opt} &= F_{opt\_peak} \times F_{opt\_frac} \\ &= \left(k_{F_{opt}} \times NDVI_{peak} + m_{F_{opt}}\right) \\ &\left(n_{F_{opt}} \times e^{\left(l_{F_{opt}} \times RDVI_{frac}\right)}\right) \end{aligned} \quad (11)$$

$$\alpha = \alpha_{peak} \times \alpha_{frac} = \left(k_\alpha \times RDVI_{peak} + m_\alpha\right) \left(n_\alpha \times e^{(l_\alpha \times RDVI_{frac})}\right), \quad (12)$$

where $k_{F_{opt}}$ and k_α are slopes and $m_{F_{opt}}$ and m_α are intercepts of the linear regressions, giving F_{opt_peak} and α_{peak}, respectively; $l_{F_{opt}}$ and l_α are coefficients and $n_{F_{opt}}$ and n_α are intercepts of the exponential regressions, giving F_{opt_frac} and α_{frac}, respectively. Equations (11) and (12) were inserted into Eq. (10), and GPP was thereby estimated as

$$\begin{aligned} GPP = &- \left(F_{opt\_peak} \times F_{opt\_frac}\right) \\ &\times \left(1 - e^{\left(\frac{-\left(\alpha_{peak} \times \alpha_{frac}\right) \times PAR}{F_{opt\_peak} \times F_{opt\_frac}}\right)}\right) = \\ &- \left(\left(k_{F_{opt}} \times NDVI_{peak} + m_{F_{opt}}\right) \left(n_{F_{opt}} \times e^{\left(l_{F_{opt}} \times RDVI_{frac}\right)}\right)\right) \\ &\times \left(1 - e^{\left(\frac{-\left(k_\alpha \times RDVI_{peak} + m_\alpha\right)\left(n_\alpha \times e^{(l_\alpha \times RDVI_{frac})}\right) \times PAR}{\left(k_{F_{opt}} \times NDVI_{peak} + m_{F_{opt}}\right)\left(l_{F_{opt}} \times RDVI_{frac} + n_{F_{opt}}\right)}\right)}\right). \end{aligned} \quad (13)$$

A bootstrap simulation methodology was used when fitting the least squares regression functions for parameterization of the GPP model (Richter et al., 2012). For each of the iterations, some of the EC site years were included and some were omitted. The bootstrap simulations generated 200 sets of $k_{F_{opt}}$, k_α, $m_{F_{opt}}$, m_α, $l_{F_{opt}}$, l_α, $n_{F_{opt}}$, n_α and coefficient of determination (R^2). Possible errors (e.g. random sampling errors, aerosols, electrical sensor noise, filtering and gap-filling errors, clouds and satellite sensor degradation) can be present in both the predictor and the response variables. Hence, we selected reduced major axis regressions to account for errors in both predictor and response variables when fitting the regression functions. The regression models were validated against the omitted site years within the bootstrap simulation methodology by calculating the RMSE and by fitting an ordinary least square linear regression between modelled and independent variables.

Similarly, the MODIS GPP product (MOD17A2H; collection 6) was evaluated against independent GPP from the EC

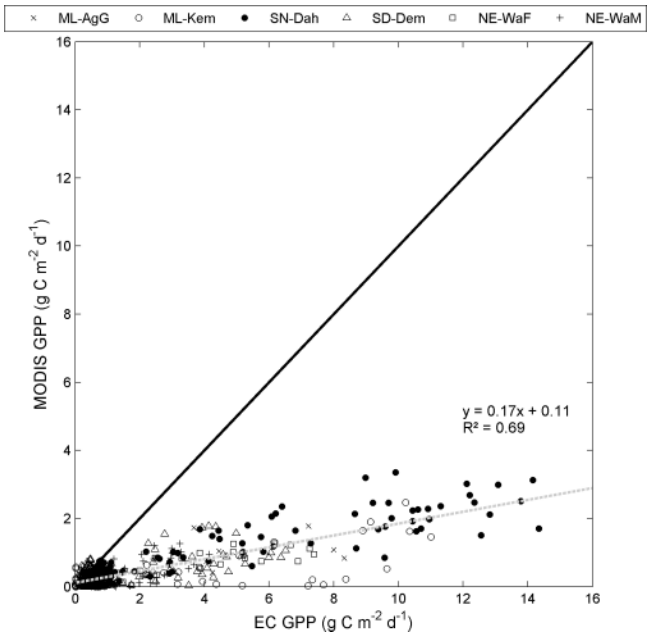

Figure 2. Evaluation of the MODIS-based GPP product MOD17A2H (collection 6) against eddy-covariance-based GPP from the six measurement sites (Fig. 1). The thick black line shows the one-to-one ratio and the grey dotted line, the fitted ordinary least squares regression.

sites by calculating the RMSE and by fitting an ordinary least square linear regression.

3 Results

3.1 Evaluation of the MODIS GPP product

There was a strong linear relationship between the MODIS GPP product (MOD17A2H; collection 6) and independent GPP (slope = 0.17; intercept = 0.11 g C m^{-2} d^{-1}; $R^2 = 0.69$; $n = 598$). However, MOD17A2H strongly underestimated independent GPP (Fig. 2), resulting in a high RMSE (2.69 g C m^{-2} d^{-1}). It can be seen that some points for the Kelma site were quite low for MOD17A2H, whereas they were relatively high for the independent GPP (Fig. 2). Kelma is an inundated Acacia forest located in a clay soil depression. These differentiated values were found in the beginning of the dry season, when the depression was still inundated, whereas the larger area was turning dry.

3.2 Intra-annual dynamics in photosynthetic capacity and quantum efficiency

Intra-annual dynamics in F_{opt} and α differed in amplitude, but were otherwise similar across the measurement sites in the Sahel (Fig. 3). There was no green ground vegetation during the dry season, and the low photosynthetic activity was due to few evergreen trees. This resulted in low values

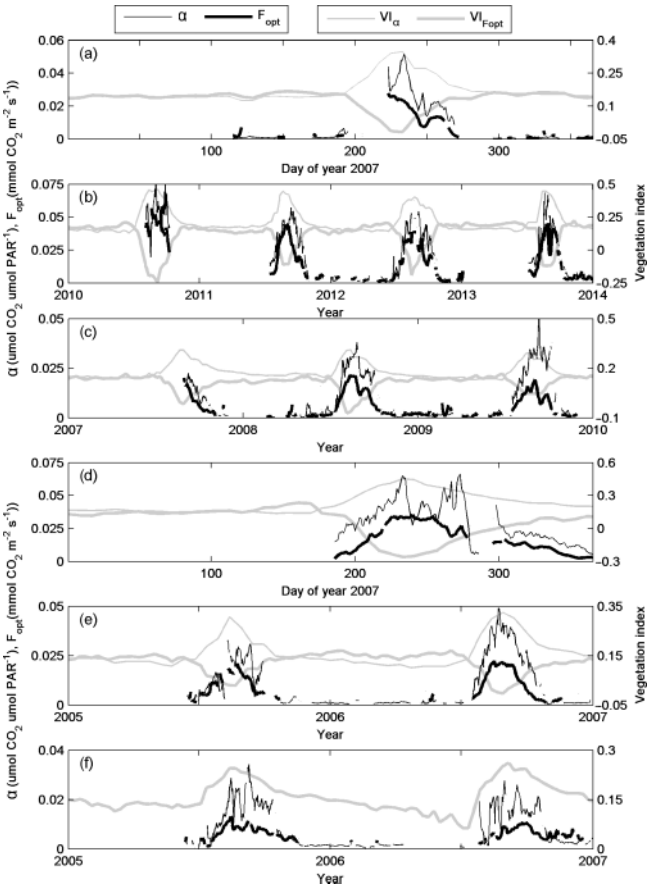

Figure 3. Time series of photosynthetic capacity (F_{opt}) and quantum efficiency (α) for the six measurement sites. Also included are time series of the vegetation indices with highest correlation with F_{opt} (VI$_{F_{opt}}$) and quantum efficiency (VI$_\alpha$; Table 2). The sites are **(a)** Agoufou (ML-AgG), **(b)** Dahra (SN-Dah), **(c)** Demokeya (SD-Dem), **(d)** Kelma (ML-Kem), **(e)** Wankama Fallow (NE-WaF) and **(f)** Wankama Millet (NE-WaM).

for both F_{opt} and α during the dry season. The vegetation responded strongly to rainfall, and both F_{opt} and α increased during the early phase of the rainy season. Generally, F_{opt} peaked slightly earlier than α (average ± 1 SD: 7 ± 10 days; Fig. 3).

All vegetation indices described intra-annual dynamics in F_{opt} reasonably well at all sites (Table 2). The vegetation index SIWSI$_{12}$ had the highest correlation for all sites except Wankama Millet, where it was RDVI. When all sites were combined, all indices described seasonality in F_{opt} well, but RDVI had the strongest correlation (Table 2).

Intra-annual dynamics in α were also closely coupled to intra-annual dynamics in the vegetation indices for all sites (Table 2). For α, RDVI was the strongest index describing intra-annual dynamics, except for Wankama Fallow, where it was EVI. When all sites were combined, all indices described intra-annual dynamics in α well, but RDVI was still the index with the strongest relationship (Table 2).

Table 2. Correlation between intra-annual dynamics in photosynthetic capacity (F_{opt}; F_{opt_frac} for all sites), quantum efficiency (α; α_{frac} for all sites) and the different vegetation indices for the six measurement sites (Fig. 1). Values are averages ±1 SD generated from 200 bootstrapping runs. The bold values are the indices with the strongest correlation. EVI is the enhanced vegetation index, NDVI is the normalized difference vegetation index, RDVI is the renormalized difference vegetation index and SIWSI is the shortwave infrared water stress index. $SIWSI_{12}$ is based on the MODIS NBAR bands 2 and 5, whereas $SIWSI_{16}$ is based on MODIS NBAR bands 2 and 6.

	F_{opt}					α				
Measurement site	EVI	NDVI	RDVI	$SIWSI_{12}$	$SIWSI_{16}$	EVI	NDVI	RDVI	$SIWSI_{12}$	$SIWSI_{16}$
ML-AgG	0.89 ± 0.02	0.87 ± 0.02	0.95 ± 0.01	**−0.95 ± 0.01**	−0.93 ± 0.02	0.92 ± 0.02	0.91 ± 0.01	**0.96 ± 0.01**	−0.94 ± 0.01	−0.88 ± 0.02
SN-Dah	0.92 ± 0.005	0.91 ± 0.01	0.96 ± 0.003	**−0.96 ± 0.004**	−0.93 ± 0.01	0.89 ± 0.01	0.90 ± 0.01	**0.93 ± 0.01**	−0.92 ± 0.01	−0.87 ± 0.01
SD-Dem	0.81 ± 0.01	0.78 ± 0.01	0.91 ± 0.01	**−0.93 ± 0.01**	−0.90 ± 0.01	0.76 ± 0.02	0.73 ± 0.02	**0.86 ± 0.01**	−0.82 ± 0.02	−0.79 ± 0.02
MA-Kem	0.77 ± 0.02	0.83 ± 0.02	0.95 ± 0.01	**−0.95 ± 0.01**	−0.90 ± 0.02	0.69 ± 0.05	0.73 ± 0.04	**0.80 ± 0.03**	−0.77 ± 0.03	−0.76 ± 0.03
NE-WaF	0.87 ± 0.02	0.81 ± 0.02	0.78 ± 0.02	**−0.90 ± 0.01**	−0.80 ± 0.02	**0.89 ± 0.01**	0.84 ± 0.01	0.85 ± 0.01	−0.88 ± 0.01	−0.79 ± 0.01
NE-WaM	0.41 ± 0.05	0.50 ± 0.04	**0.72 ± 0.03**	−0.55 ± 0.04	−0.43 ± 0.05	0.72 ± 0.02	0.76 ± 0.02	**0.81 ± 0.01**	−0.75 ± 0.01	−0.72 ± 0.01
All sites	0.86 ± 0.0	0.79 ± 0.0	**0.90 ± 0.0**	0.75 ± 0.0	0.70 ± 0.0	0.83 ± 0.01	0.80 ± 0.01	**0.86 ± 0.01**	0.62 ± 0.01	0.54 ± 0.01

Table 3. Statistics for the regression tree analysis. Regression tree analysis was used to study relationships between intra-annual dynamics in photosynthetic capacity (F_{opt}; F_{opt_frac} for all sites) and quantum efficiency (α; α_{frac} for all sites) and explanatory variables. The pruning level is the number of splits of the regression tree and an indication of complexity of the system.

Measurement site	Explanatory variables					Pruning level	R^2
F_{opt}	1	2	3	4	5		
ML-AgG	$SIWSI_{12}$	Tair	PAR	SWC		16	0.98
SN-Dah	$SIWSI_{12}$	SWC	VPD	Tair	PAR	84	0.98
SD-Dem	$SIWSI_{12}$	VPD	SWC	Tair	PAR	33	0.97
ML-Kem	$SIWSI_{12}$	PAR	Tair	VPD		22	0.98
NE-WaF	$SIWSI_{12}$	SWC	VPD	Tair		14	0.92
NE-WaM	RDVI	SWC	VPD	Tair		18	0.75
All sites	RDVI	SWC	Tair	VPD		16	0.87
α							
ML-AgG	RDVI					3	0.95
SN-Dah	RDVI	VPD	SWC	Tair	PAR	21	0.93
SD-Dem	RDVI	SWC	PAR	Tair		16	0.93
ML-Kem	RDVI	Tair				4	0.75
NE-WaF	EVI	SWC	VPD			10	0.90
NE-WaM	RDVI	SWC	VPD	Tair		15	0.86
All sites	RDVI	SWC	VPD	Tair		16	0.84

The regression trees used for gap-filling explained the intra-annual dynamics in F_{opt} and α well for all sites (Table 3; Fig. S2). The regression trees explained intra-annual dynamics in F_{opt} better than in α, and multi-year sites were better predicted than single-year sites (Fig. S2). The main explanatory variables coupled to intra-annual dynamics in F_{opt} for all sites across the Sahel were on the order of RDVI, SWC, VPD, T_{air} and PAR. For α, they were RDVI, SWC, VPD and T_{air} (Table 3). The strong relationship to SWC and VPD indicates drought stress during periods of low rainfall. For all sites across the Sahel, incorporating hydrometeorological variables increased the ability to determine intra-annual dynamics in F_{opt} and α compared to the ordinary least square linear regressions against vegetation indices (Table 2, data given as r; Table 3; Figs. 3 and S2). For all sites, incorporation of these variables increased R^2 from 0.81 to 0.87 and from 0.74 to 0.84 for F_{opt} and α, respectively.

3.3 Spatial and inter-annual dynamics in photosynthetic capacity and quantum efficiency

Large spatial and inter-annual variability in F_{opt_peak} and α_{peak} were found across the six measurement sites; F_{opt_peak} ranged between 10.1 (Wankama Millet 2005) and 50.0 µmol CO_2 m^{-2} s^{-1} (Dahra 2010), and α_{peak} ranged between 0.020 (Demokeya 2007) and 0.064 µmol CO_2 µmol PAR^{-1} (Dahra 2010; Table 4). The average 2-week running mean peak values of F_{opt} and α for all sites were 26.4 µmol CO_2 m^{-2} s^{-1} and 0.040 µmol CO_2 µmol PAR^{-1}, respectively. All vegetation

Table 4. Annual peak values of quantum efficiency (α_{peak}; µmol CO_2 µmol PAR^{-1}) and photosynthetic capacity (F_{opt_peak}; µmol CO_2 m^{-2} s^{-1}) for the six measurement sites (Fig. 1). The peak values are the 2-week running mean with highest annual value.

Measurement site	Year	α_{peak}	F_{opt_peak}
ML-AgG	2007	0.0396	24.5
SN-Dah	2010	0.0638	50.0
	2011	0.0507	42.3
	2012	0.0480	39.2
	2013	0.0549	40.0
SD-Dem	2007	0.0257	16.5
	2008	0.0327	21.0
	2009	0.0368	16.5
ML-Kem	2007	0.0526	33.5
NE-WaF	2005	0.0273	18.2
	2006	0.0413	21.0
NE-WaM	2005	0.0252	10.6
	2006	0.0200	10.1
Average		0.0399	26.4

indices determined spatial and inter-annual dynamics well in both F_{opt_peak} and α_{peak} (Table 5); F_{opt_peak} was most closely coupled with $NDVI_{peak}$, whereas α_{peak} was more closely coupled with $RDVI_{peak}$ (Fig. 4). F_{opt_peak} also correlated well with peak dry weight biomass, C content in the soil and RH, whereas α_{peak} also correlated with peak dry weight biomass and C content in the soil (Table 5).

3.4 Spatially extrapolated photosynthetic capacity, quantum efficiency and gross primary production across the Sahel and evaluation of the GPP model

The spatially extrapolated F_{opt}, α and GPP averaged over the Sahel for 2001–2014 were 22.5 ± 1.7 µmol CO_2 m^{-2} s^{-1}, 0.030 ± 0.002 µmol CO_2 µmol PAR^{-1} and 736 ± 39 g C m^{-2} yr^{-1}, respectively. At a regional scale, it can be seen that F_{opt}, α and GPP decreased substantially with latitude (Fig. 5). The highest values were found in south-eastern Senegal, western Mali, in parts of southern Sudan and on the border between Sudan and South Sudan. The lowest values were found along the northernmost parts of the Sahel on the border to the Sahara in Mauritania, in northern Mali and in northern Niger.

Modelled GPP was similar to independent GPP on average, and there was a strong linear relationship between modelled GPP and independent GPP for all sites (Fig. 6; Table 6). However, when separating the evaluation between measurement sites, it can be seen that the model reproduced some sites better than others (Fig. 7; Table 6). Wankama Millet was generally overestimated, whereas on average the model worked well for Demokeya but underestimated high values (Fig. 7; Table 6). Variability of independent GPP at the other sites was reproduced by the model reasonably well (Fig. 7; Table 6). The final parameters of the GPP model (Eq. 13) are shown in Table 7.

Table 5. Correlation matrix between annual peak values of photosynthetic capacity (F_{opt_peak}) and quantum efficiency (α_{peak}) and measured environmental variables: annual rainfall (P); yearly averages of air temperature at 2 m height (T_{air}), soil water content measured at 0.1 m depth (SWC; % volumetric water content), relative humidity (Rh), vapour pressure deficit (VPD) and incoming global radiation (R_g); soil nitrogen (N) and carbon (C) contents; and annual peak values of the normalized difference vegetation index ($NDVI_{peak}$), the enhanced vegetation index (EVI_{peak}), the renormalized difference vegetation index ($RDVI_{peak}$), the shortwave infrared water stress index based on MODIS NBAR bands 2 and 5 ($SIWSI_{12peak}$), and the SIWSI based on MODIS NBAR bands 2 and 6 ($SIWSI_{16peak}$). Sample size was 13 for all except the marked explanatory variables.

Explanatory variable	F_{opt_peak}	α_{peak}
Meteorological data		
P (mm)	0.24 ± 0.26	0.13 ± 0.27
T_{air} (°C)	-0.07 ± 0.25	-0.01 ± 0.25
SWC (%)[a]	0.33 ± 0.25	0.16 ± 0.27
Rh (%)	0.73 ± 0.16*	0.60 ± 0.19
VPD (hPa)	0.20 ± 0.26	0.15 ± 0.30
R_g (W m^{-2})	-0.48 ± 0.21	-0.41 ± 0.24
Biomass and edaphic data		
Biomass (g DW m^{-2})[a]	0.77 ± 0.15*	0.74 ± 0.14*
C3 / C4 ratio	-0.05 ± 0.26	0.06 ± 0.30
N cont. (%)[b]	0.22 ± 0.11	0.35 ± 0.14
C cont. (%)[b]	0.89 ± 0.06**	0.87 ± 0.07**
Earth observation data		
$NDVI_{peak}$	0.94 ± 0.05**	0.87 ± 0.07**
EVI_{peak}	0.93 ± 0.04**	0.87 ± 0.07**
$RDVI_{peak}$	0.93 ± 0.04**	0.89 ± 0.07**
$SIWSI_{12peak}$	0.85 ± 0.08**	0.84 ± 0.08**
$SIWSI_{16peak}$	0.67 ± 0.12*	0.65 ± 0.15*
Photosynthetic variables		
F_{opt}	–	0.94 ± 0.03**

[a] Sample size equals 11. [b] Sample size equals 9. * Significant at 0.05 level. ** Significant at 0.01 level.

4 Discussion

Our hypothesis that vegetation indices closely related to SIWSI would be most strongly coupled with intra-annual dynamics in F_{opt} and α was not rejected for F_{opt} since this was the case for all sites except for Wankama Millet (Table 2). However, our hypothesis was rejected for α, since it was more closely related to vegetation indices of chlorophyll

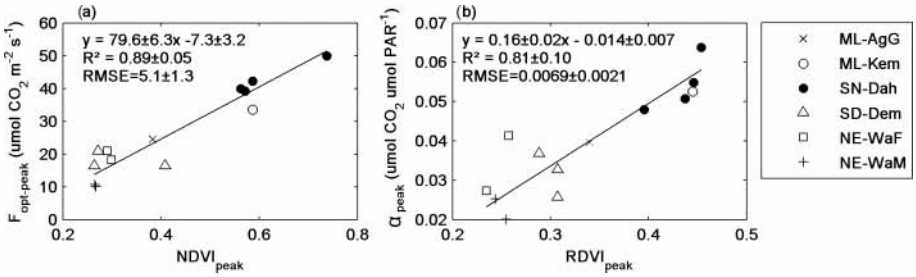

Figure 4. Scatter plots of annual peak values for the six measurement sites (Fig. 1) of **(a)** photosynthetic capacity ($F_{\text{opt\_peak}}$) and **(b)** quantum efficiency (α_{peak}) against peak values of normalized difference vegetation index ($\text{NDVI}_{\text{peak}}$) and renormalized difference vegetation index ($\text{RDVI}_{\text{peak}}$), respectively. The annual peak values were estimated by taking the annual maximum of a 2-week running mean.

Table 6. Statistics regarding the evaluation of the gross primary production (GPP) model for the six measurement sites (Fig. 1). In situ and modelled GPP are averages ±1 SD. RMSE is the root mean square error, and slope, intercept and R^2 are from the fitted ordinary least square linear regressions.

Measurement site	In situ GPP ($\mu\text{mol CO}_2\ \text{m}^{-2}\ \text{s}^{-1}$)	Modelled GPP ($\mu\text{mol CO}_2\ \text{m}^{-2}\ \text{s}^{-1}$)	RMSE ($\mu\text{mol CO}_2\ \text{m}^{-2}\ \text{s}^{-1}$)	Slope	Intercept ($\mu\text{mol CO}_2\ \text{m}^{-2}\ \text{s}^{-1}$)	R^2
ML-AgG	5.35 ± 6.38	5.97 ± 5.80	2.48 ± 0.10	0.84 ± 0.003	1.46 ± 0.01	0.86 ± 0.002
SN-Dah	9.39 ± 10.17	8.87 ± 9.67	3.99 ± 1.34	0.88 ± 0.002	0.62 ± 0.01	0.85 ± 0.001
SD-Dem	4.26 ± 4.55	3.98 ± 3.90	3.15 ± 1.06	0.63 ± 0.003	1.31 ± 0.007	0.54 ± 0.02
ML-Kem	11.16 ± 8.02	10.52 ± 9.22	4.35 ± 1.23	1.02 ± 0.003	−0.82 ± 0.03	0.78 ± 0.002
NE-WaF	5.77 ± 4.17	6.63 ± 3.53	2.47 ± 1.05	0.70 ± 0.005	2.58 ± 0.02	0.69 ± 0.003
NE-WaM	3.04 ± 1.93	6.35 ± 3.47	4.12 ± 0.99	1.31 ± 0.004	2.37 ± 0.02	0.53 ± 0.003
Average	6.73 ± 7.72	7.02 ± 7.39	3.68 ± 0.55	0.83 ± 0.07	1.34 ± 0.82	0.84 ± 0.07

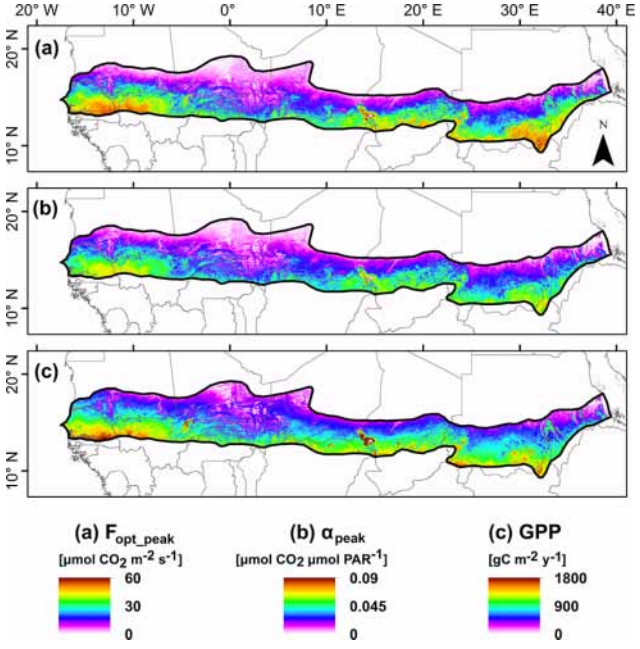

Figure 5. Maps of **(a)** peak values of photosynthetic capacity ($F_{\text{opt\_peak}}$) averaged for 2001–2014, **(b)** peak values of quantum efficiency (α_{peak}) averaged for 2001–2014 and **(c)** annual budgets of GPP averaged for 2001–2014.

Table 7. The parameters for Eq. (13) that were used in the final gross primary production (GPP) model. RMSE is the root mean square error, and R^2 is the coefficient of determination for the regression models predicting the different variables.

Parameter	Value	RMSE	R^2
$k_{F_{\text{opt}}}$	79.6 ± 6.3	5.1 ± 1.3	0.89 ± 0.05
$m_{F_{\text{opt}}}$	−7.3 ± 3.2		
$l_{F_{\text{opt}}}$	3.51 ± 0.19	0.15 ± 0.02	0.88 ± 0.06
$n_{F_{\text{opt}}}$	0.03 ± 0.006		
α	0.16 ± 0.02	0.0069 ± 0.0021	0.81 ± 0.10
$m_{F_{\text{opt}}}$	−0.014 ± 0.007		
$l_{F_{\text{opt}}}$	3.75 ± 0.27	0.20 ± 0.02	0.80 ± 0.10
$n_{F_{\text{opt}}}$	0.02 ± 0.007		

abundance (RDVI and EVI). In the Sahel, soil moisture conditions in the early rainy season are important for vegetation growth, and during this phase vegetation is especially vulnerable to drought conditions (Rockström and de Rouw, 1997; Tagesson et al., 2016a; Mbow et al., 2013). Photosynthetic capacity (F_{opt}) peaked earlier than α did in the rainy season (Fig. 3), thereby explaining the close relationship of F_{opt} to SIWSI. Leaf area index increased over the growing season and leaf area index is closely coupled with vegetation indices related to chlorophyll abundance (Tagesson et al., 2009). The

increase in leaf area index increased canopy level quantum efficiency (α), thereby explaining the closer relationship of α with RDVI.

Our hypothesis that vegetation indices closely related to chlorophyll abundance would be most strongly coupled with spatial and inter-annual dynamics in F_{opt} and α was not rejected for either F_{opt} or α; NDVI, EVI and RDVI all correlated with spatial and inter-annual dynamics in F_{opt} and α (Table 5). However, it was surprising that $NDVI_{peak}$ had the strongest correlation with spatial and inter-annual variability in F_{opt} (Table 5). Both EVI and RDVI should be less sensitive to saturation effects than NDVI (Huete et al., 2002; Roujean and Breon, 1995), and based on this it can be assumed that peak values of these indices should have stronger relationships with peak values of F_{opt} and α. However, vegetation indices with a high sensitivity to changes in green biomass at high biomass loads become less sensitive to green biomass changes at low biomass loads (Huete et al., 2002). The peak leaf area index for ecosystems across the Sahel is generally $\sim 2\,m^2\,m^{-2}$ or less, whereas the saturation issue of NDVI generally starts at a leaf area index of about 2–5 $m^2\,m^{-2}$ (Haboudane et al., 2004).

The F_{opt_peak} estimates from Agoufou, Demokeya and the Wankama sites were similar, whereas Dahra and Kelma values were high in relation to previously reported canopy-scale F_{opt_peak} from the Sahel (~ -8 to $-23\,\mu mol\,m^{-2}\,s^{-1}$; Hanan et al., 1998; Merbold et al., 2009; Moncrieff et al., 1997; Boulain et al., 2009; Levy et al., 1997; Monteny et al., 1997). These previous studies reported much lower F_{opt} at canopy scale than at leaf scale (e.g. Levy et al., 1997: 10 vs. $44\,\mu mol\,m^{-2}\,s^{-1}$; Boulain et al., 2009: 8 vs. $50\,\mu mol\,m^{-2}\,s^{-1}$). The leaf area index at Dahra and Kelma peaked at 2.1 and 2.7, respectively (Timouk et al., 2009; Tagesson et al., 2015a), and it was substantially higher than at the above-mentioned sites. A possible explanation for high F_{opt} estimates at Dahra and Kelma could therefore be the higher leaf area index. Tagesson et al. (2016b) performed a quality check of the EC data due to the high net CO_2 exchange measured at the Dahra field site and explained the high values by a combination of moderately dense herbaceous C4 ground vegetation, high soil nutrient availability and a grazing pressure resulting in compensatory growth and fertilization effects. Another possible explanation could be that the West African monsoon brings a humid layer of surface air from the Atlantic, possibly increasing vegetation production for the most western part of the Sahel (Tagesson et al., 2016a).

Our model substantially overestimated GPP for Wankama Millet (Fig. 7f). Being a crop field, this site differed from the other sites in its species composition and ecosystem structure, as well as land and vegetation management. Crop fields in southwestern Niger are generally characterized by rather low production, resulting from decreased fertility and soil loss caused by intensive land use (Cappelaere et al., 2009). These specifics of the Wankama Millet site may cause the model, parameterized with observations from the other study sites without this strong anthropogenic influence, to overestimate GPP at this site. Similar results were found by Boulain et al. (2009) when applying an upscaling model using leaf area index for Wankama Millet and Wankama Fallow. It worked well for Wankama fallow, whereas it was less conclusive for Wankama Millet. The main explanation for this difference was low leaf area index in millet fields because of a low density of millet stands due to agricultural practice. There is extensive savanna clearing for food production in the Sahel (Leblanc et al., 2008; Boulain et al., 2009; Cappelaere et al., 2009). To further understand impacts of this land cover change on vegetation production and land–atmosphere exchange processes, there is an urgent need for more study sites covering cropped areas in this region.

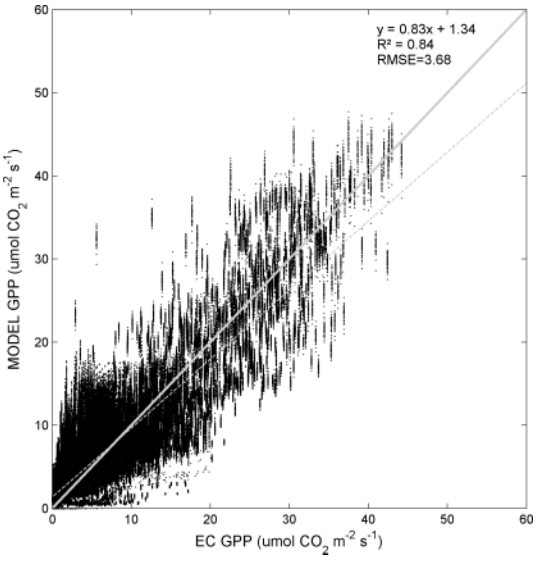

Figure 6. Evaluation of the modelled gross primary production (GPP; Eq. 13) against in situ GPP from all six measurement sites. The thick grey line shows the one-to-one ratio, whereas the thin dotted grey line is the fitted ordinary least square regression.

In Demokeya, GPP was slightly underestimated for 2008 (Fig. 7c) because modelled F_{opt} was much lower than the actual measured value in 2008 (the thick black line in Fig. 4). An improvement of the model could be to incorporate some parameters that constrain or enhance F_{opt} depending on environmental stress. Indeed, the regression tree analysis indicated that incorporating hydrometeorological variables increased the ability to predict both F_{opt} and α. Conversely, for spatial upscaling purposes, it has been shown that including modelled hydrometeorological constraints on LUE decreases the ability to predict vegetation production due to the incorporated uncertainty in these modelled variables (Fensholt et al., 2006; Ma et al., 2014). For spatial upscaling to regional scales, it is therefore better to simply use relationships with EO data. This is particularly the case for the Sahel, one of the

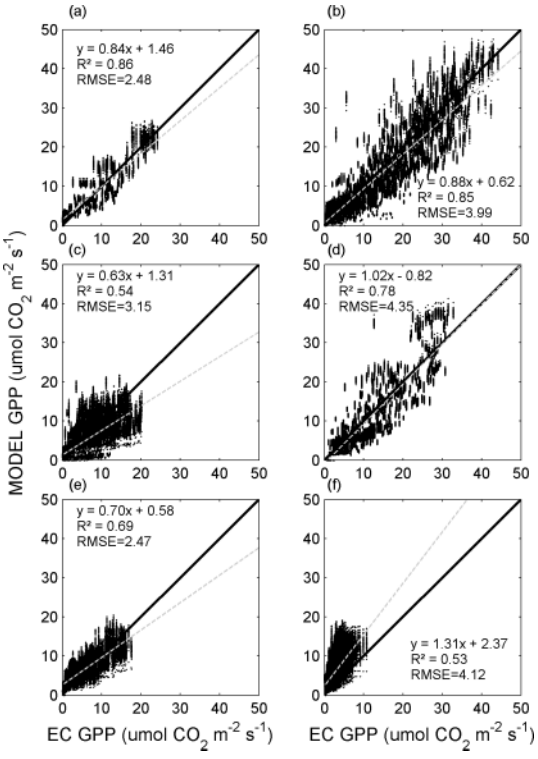

Figure 7. Evaluation of the modelled gross primary production (GPP; Eq. 13) against in situ GPP for the six sites across the Sahel (Fig. 1). The thick black lines show the one-to-one ratios, whereas the dotted thin grey lines are the fitted ordinary least square regressions. The sites are **(a)** Agoufou (ML-AgG), **(b)** Dahra (SN-Dah), **(c)** Demokeya (SD-Dem), **(d)** Kelma (ML-Kem), **(e)** Wankama Fallow (NE-WaF) and **(f)** Wankama Millet (NE-WaM).

largest dryland areas in the world, which includes only a few sites of hydrometeorological observations.

The pattern seen in the spatially explicit GPP budgets (Fig. 5c) may be influenced by a range of biophysical and anthropogenic factors. The clear north–south gradient is expected given the strong north–south rainfall gradient in the Sahel. The West African monsoon mentioned above could also be an explanation of high GPP values in the western part of the Sahel, where values were relatively high in relation to GPP at similar latitudes in the central and eastern Sahel (Fig. 5c). The areas with the highest GPP are sparsely populated woodlands or shrubby savanna with a relatively dense tree cover (Brandt et al., 2016). However, the maps produced here should be used with caution as they are based on upscaling of data collected at only six EC sites available in the region, especially given the issues related to the cropped fields discussed earlier. Still, the average GPP budget for the entire Sahel 2001–2014 was close to an average annual GPP budget estimated at these six sites ($692 \pm 89\,\mathrm{g\,C\,m^{-2}\,yr^{-1}}$; Tagesson et al., 2016a). The range of GPP budgets in Fig. 5c is also similar to previous annual GPP budgets reported from other savannas across the world (Veenendaal et al., 2004; Chen et al., 2003, 2006; Kanniah et al., 2010).

Although MOD17A2 GPP has previously been shown to capture GPP in several ecosystems types well (Turner et al., 2006, 2005; Heinsch et al., 2006; Sims et al., 2006; Kanniah et al., 2009), it has been shown to underestimate it in others (Coops et al., 2007; Gebremichael and Barros, 2006; Sjöström et al., 2013). Gross primary production of Sahelian drylands have not been captured well by MOD17A2 (Sjöström et al., 2013; Fensholt et al., 2006), and as we have shown, this underestimation persists in the latest MOD17A2H GPP (collection 6) product (Fig. 2). The main reason for this pronounced underestimation is that maximum LUE is set to $0.84\,\mathrm{g\,C\,MJ^{-1}}$ (open shrubland, Demokeya) and $0.86\,\mathrm{g\,C\,MJ^{-1}}$ (grassland; Agoufou, Dahra, Kelma; Wankama Millet and Wankama Fallow) in the BPLUT, i.e. much lower than maximum LUE measured at the Sahelian measurement sites of this study (average: $2.47\,\mathrm{g\,C\,MJ^{-1}}$; range: 1.58–$3.50\,\mathrm{g\,C\,MJ^{-1}}$; Sjöström et al., 2013; Tagesson et al., 2015a), a global estimate of $\sim 1.5\,\mathrm{g\,C\,MJ^{-1}}$ (Garbulsky et al., 2010) and a savanna site in Australia ($1.26\,\mathrm{g\,C\,MJ^{-1}}$; Kanniah et al., 2009).

Several dynamic global vegetation models have been used for decades to quantify GPP at different spatial and temporal scales (Dickinson, 1983; Sellers et al., 1997). These models are generally based on the photosynthesis model of Farquhar et al. (1980), a model particularly sensitive to uncertainty in photosynthetic capacity (Zhang et al., 2014). This and several previous studies have shown that both photosynthetic capacity and efficiency (both α and LUE) can vary considerably between seasons as well as spatially vary, and both within and between vegetation types (Eamus et al., 2013; Garbulsky et al., 2010; Ma et al., 2014; Tagesson et al., 2015a). This variability is difficult to estimate using broad values based on land cover classes, yet most models apply a constant value, which can cause substantial inaccuracies in the estimates of seasonal and spatial variability in GPP. This is particularly a problem in savannas that consist of several plant functional types (C3 and C4 species, and a large variability in tree and/or herbaceous vegetation fractions; Scholes and Archer, 1997). This study indicates the applicability of EO as a tool for parameterizing spatially explicit estimates of plant physiological variables, which could improve our ability to simulate GPP. Spatially explicit estimates of GPP at a high temporal and spatial resolution are essential for environmental change studies in the Sahel and can contribute to increased knowledge regarding changes in GPP, its relationship to climatic change and anthropogenic forcing, and simulations of ecosystem processes and hydro-biochemical cycles.

Data availability. The EC data are available from Fluxnet (http://fluxnet.ornl.gov) and CarboAfrica (http://www.carboafrica.net/indexen.asp). The ERA Interim PAR data are available from ECMWF (http://apps.ecmwf.int/datasets/data/interim-full-daily/

levtype=sfc/). The data products from this study are available from the corresponding author upon request.

The Supplement related to this article is available online at doi:10.5194/bg-14-1333-2017-supplement.

Competing interests. The authors declare that they have no conflict of interest.

Acknowledgements. Data are available from Fluxnet (http://fluxnet.ornl.gov) and CarboAfrica (http://www.carboafrica.net/indexen.asp). Data for the Mali and Niger sites were made available by the AMMA-CATCH regional observatory (www.amma-catch.org), which is funded by the French Institut de Recherche pour le Développement (IRD) and Institut National des Sciences de l'Univers (INSU). The project was funded by the Danish Council for Independent Research (DFF) Sapere Aude programme. The Faculty of Science, Lund University supported the Dahra and Demokeya measurements with an infrastructure grant. Torbern Tagesson and Jonas Ardö received support from the Swedish National Space Board. We would like to thank the editor Charles Bourque, the reviewer Niall Hanan and the anonymous reviewer for a very constructive and thorough critique that significantly helped improve the paper.

Edited by: C. Bourque
Reviewed by: N. P. Hanan and one anonymous referee

References

Abdi, A., Seaquist, J., Tenenbaum, D., Eklundh, L., and Ardö, J.: The supply and demand of net primary production in the Sahel, Environ. Res. Lett., 9, 1–11, doi:10.1088/1748-9326/9/9/094003, 2014.

Ahlström, A., Raupach, M. R., Schurgers, G., Smith, B., Arneth, A., Jung, M., Reichstein, M., Canadell, J. G., Friedlingstein, P., Jain, A. K., Kato, E., Poulter, B., Sitch, S., Stocker, B. D., Viovy, N., Wang, Y. P., Wiltshire, A., Zaehle, S., and Zeng, N.: The dominant role of semi-arid ecosystems in the trend and variability of the land CO_2 sink, Science, 348, 895–899, doi:10.1126/science.aaa1668, 2015.

Baldocchi, D., Falge, E., Gu, L., Olson, R., Hollinger, D., Running, S., Anthoni, P., Bernhofer, C., Davis, K., Evans, R., Fuentes, J., Goldstein, A., Katul, G., Law, B., Lee, X., Malhi, Y., Meyers, T., Munger, W., Oechel, W., Paw, K. T., Pilegaard, K., Schmid, H. P., Valentini, R., Verma, S., Vesala, T., Wilson, K., and Wofsy, S.: FLUXNET: A New Tool to Study the Temporal and Spatial Variability of Ecosystem–Scale Carbon Dioxide, Water Vapor, and Energy Flux Densities, B. Am. Meteorol. Soc., 82, 2415–2434, doi:10.1175/1520-0477(2001)082<2415:fantts>2.3.co;2, 2001.

Boulain, N., Cappelaere, B., Ramier, D., Issoufou, H. B. A., Halilou, O., Seghieri, J., Guillemin, F., Oï, M., Gignoux, J., and Timouk, F.: Towards an understanding of coupled physical and biological processes in the cultivated Sahel – 2. Vegetation and carbon dynamics, J. Hydrol., 375, 190–203, doi:10.1016/j.jhydrol.2008.11.045, 2009.

Brandt, M., Hiernaux, P., Rasmussen, K., Mbow, C., Kergoat, L., Tagesson, T., Ibrahim, Y. Z., Wélé, A., Tucker, C. J., and Fensholt, R.: Assessing woody vegetation trends in Sahelian drylands using MODIS based seasonal metrics, Remote Sens. Environ., 183, 215–225, doi:10.1016/j.rse.2016.05.027, 2016.

Broge, N. H. and Leblanc, E.: Comparing prediction power and stability of broadband and hyperspectral vegetation indices for estimation of green leaf area index and canopy chlorophyll density, Remote Sens. Environ., 76, 156–172, doi:10.1016/S0034-4257(00)00197-8, 2001.

Cannell, M. and Thornley, J.: Temperature and CO_2 Responses of Leaf and Canopy Photosynthesis: a Clarification using the Non-rectangular Hyperbola Model of Photosynthesis, Ann. Bot., 82, 883–892, 1998.

Cappelaere, B., Descroix, L., Lebel, T., Boulain, N., Ramier, D., Laurent, J. P., Favreau, G., Boubkraoui, S., Boucher, M., Bouzou Moussa, I., Chaffard, V., Hiernaux, P., Issoufou, H. B. A., Le Breton, E., Mamadou, I., Nazoumou, Y., Oi, M., Ottlé, C., and Quantin, G.: The AMMA-CATCH experiment in the cultivated Sahelian area of south-west Niger – Investigating water cycle response to a fluctuating climate and changing environment, J. Hydrol., 375, 34–51, doi:10.1016/j.jhydrol.2009.06.021, 2009.

Chen, C., Cleverly, J., and Zhang, L.: Modelling Seasonal and Interannual Variations in Carbon and Water Fluxes in an Arid-Zone Acacia Savanna Woodland, 1981–2012, Ecosystems, 19, 625–644, 2016.

Chen, X., Hutley, L., and Eamus, D.: Carbon balance of a tropical savanna of northern Australia, Oecologia, 137, 405–416, 2003.

Coops, N. C., Black, T. A., Jassal, R. S., Trofymow, J. A., and Morgenstern, K.: Comparison of MODIS, eddy covariance determined and physiologically modelled gross primary production (GPP) in a Douglas-fir forest stand, Remote Sens. Environ., 107, 385–401, doi:10.1016/j.rse.2006.09.010, 2007.

Dardel, C., Kergoat, L., Hiernaux, P., Mougin, E., Grippa, M., and Tucker, C. J.: Re-greening Sahel: 30 years of remote sensing data and field observations (Mali, Niger), Remote Sens. Environ., 140, 350–364, doi:10.1016/j.rse.2013.09.011, 2014.

De'ath, G. and Fabricius, K. E.: Classification and regression trees: A powerful yet simple technique for ecological data analysis, Ecology, 81, 3178–3192, doi:10.2307/177409, 2000.

de Ridder, N., Stroosnijder, L., and Cisse, A. M.: Productivity of Sahelian rangelands: a study of the soils, the vegetations and the exploitation of that natural resource, PPS course book, Primary Production in the Sahel, Agricultural University, Wageningen, 1982.

Dee, D. P., Uppala, S. M., Simmons, A. J., Berrisford, P., Poli, P., Kobayashi, S., Andrae, U., Balmaseda, M. A., Balsamo, G., Bauer, P., Bechtold, P., Beljaars, A. C. M., van de Berg, L., Bidlot, J., Bormann, N., Delsol, C., Dragani, R., Fuentes, M., Geer, A. J., Haimberger, L., Healy, S. B., Hersbach, H., Hólm, E. V., Isaksen, L., Kållberg, P., Köhler, M., Matricardi, M., McNally, A. P., Monge-Sanz, B. M., Morcrette, J. J., Park, B. K., Peubey, C., de Rosnay, P., Tavolato, C., Thépaut, J. N., and Vitart, F.: The ERA-Interim reanalysis: configuration and performance of the data assimilation system, Q. J. Roy. Meteorol. Soc., 137, 553–597, doi:10.1002/qj.828, 2011.

Dickinson, R. E.: Land Surface Processes and Climate–Surface Albedos and Energy Balance, in: Advances in Geophysics, edited by: Barry, S., Elsevier, 305–353, 1983.

Eamus, D., Cleverly, J., Boulain, N., Grant, N., Faux, R., and Villalobos-Vega, R.: Carbon and water fluxes in an arid-zone Acacia savanna woodland: An analyses of seasonal patterns and responses to rainfall events, Agr. Forest Meteorol., 182–183, 225–238, doi:10.1016/j.agrformet.2013.04.020, 2013.

ECMWF: ERA Interim Daily: http://apps.ecmwf.int/datasets/data/interim-full-daily/levtype=sfc/, last access: 4 April 2016a.

ECMWF: ERA-Interim: surface photosynthetically active radiation (surface PAR) values are too low, available at: https://software.ecmwf.int/wiki/display/CKB, last access: 7 November 2016b.

Falge, E., Baldocchi, D., Olson, R., Anthoni, P., Aubinet, M., Bernhofer, C., Burba, G., Ceulemans, R., Clement, R., Dolman, H., Granier, A., Gross, P., Grunwald, T., Hollinger, D., Jensen, N. O., Katul, G., Keronen, P., Kowalski, A., Lai, C. T., Law, B. E., Meyers, T., Moncrieff, J. B., Moors, E., Munger, J. W., Pilegaard, K., Rannik, U., Rebmann, C., Suyker, A., Tenhunen, J., Tu, K., Verma, S., Vesala, T., Wilson, K., and Wofsy, S.: Gap filling strategies for defensible annual sums of net ecosystem exchange, Agr. Forest Meteorol., 107, 43–69, 2001.

Farquhar, G. D., Caemmerer, S., and Berry, J. A.: A biochemical model of photosynthetic CO_2 assimilation in leaves of C3 plants, Planta, 149, 78–90, 1980.

Fensholt, R. and Sandholt, I.: Derivation of a shortwave infrared water stress index from MODIS near- and shortwave infrared data in a semiarid environment, Remote Sens. Environ., 87, 111–121, doi:10.1016/j.rse.2003.07.002, 2003.

Fensholt, R., Sandholt, I., Rasmussen, M. S., Stisen, S., and Diouf, A.: Evaluation of satellite based primary production modelling in the semi-arid Sahel, Remote Sens. Environ., 105, 173–188, doi:10.1016/j.rse.2006.06.011, 2006.

Fensholt, R., Rasmussen, K., Kaspersen, P., Huber, S., Horion, S., and Swinnen, E.: Assessing Land Degradation/Recovery in the African Sahel from Long-Term Earth Observation Based Primary Productivity and Precipitation Relationships, Remote Sensing, 5, 664–686, 2013.

Garbulsky, M. F., Peñuelas, J., Papale, D., Ardö, J., Goulden, M. L., Kiely, G., Richardson, A. D., Rotenberg, E., Veenendaal, E. M., and Filella, I.: Patterns and controls of the variability of radiation use efficiency and primary productivity across terrestrial ecosystems, Global Ecol. Biogeogr., 19, 253–267, doi:10.1111/j.1466-8238.2009.00504.x, 2010.

Gates, D. M., Keegan, H. J., Schleter, J. C., and Weidner, V. R.: Spectral Properties of Plants, Appl. Opt., 4, 11–20, 1965.

Gebremichael, M. and Barros, A. P.: Evaluation of MODIS Gross Primary Productivity (GPP) in tropical monsoon regions, Remote Sens. Environ., 100, 150–166, doi:10.1016/j.rse.2005.10.009, 2006.

Haboudane, D., Miller, J. R., Pattey, E., Zarco-Tejada, P. J., and Strachan, I. B.: Hyperspectral vegetation indices and novel algorithms for predicting green LAI of crop canopies: Modeling and validation in the context of precision agriculture, Remote Sens. Environ., 90, 337–352, doi:10.1016/j.rse.2003.12.013, 2004.

Hanan, N., Kabat, P., Dolman, J., and Elbers, J. A. N.: Photosynthesis and carbon balance of a Sahelian fallow savanna, Glob. Change Biol., 4, 523–538, 1998.

Heinsch, F. A., Maosheng, Z., Running, S. W., Kimball, J. S., Nemani, R. R., Davis, K. J., Bolstad, P. V., Cook, B. D., Desai, A. R., Ricciuto, D. M., Law, B. E., Oechel, W. C., Hyojung, K., Hongyan, L., Wofsy, S. C., Dunn, A. L., Munger, J. W., Baldocchi, D. D., Liukang, X., Hollinger, D. Y., Richardson, A. D., Stoy, P. C., Siqueira, M. B. S., Monson, R. K., Burns, S. P., and Flanagan, L. B.: Evaluation of remote sensing based terrestrial productivity from MODIS using regional tower eddy flux network observations, IEEE T. Geosci. Remote, 44, 1908–1925, doi:10.1109/TGRS.2005.853936, 2006.

Hickler, T., Eklundh, L., Seaquist, J. W., Smith, B., Ardö, J., Olsson, L., Sykes, M. T., and Sjöström, M.: Precipitation controls Sahel greening trend, Geophys. Res. Lett., 32, L21415, doi:10.1029/2005GL024370, 2005.

Huber, S., Tagesson, T., and Fensholt, R.: An automated field spectrometer system for studying VIS, NIR and SWIR anisotropy for semi-arid savanna, Remote Sens. Environ., 152, 547–556, 2014.

Huete, A., Didan, K., Miura, T., Rodriguez, E. P., Gao, X., and Ferreira, L. G.: Overview of the radiometric and biophysical performance of the MODIS vegetation indices, Remote Sens. Environ., 83, 195–213, 2002.

Ide, R., Nakaji, T., and Oguma, H.: Assessment of canopy photosynthetic capacity and estimation of GPP by using spectral vegetation indices and the light-response function in a larch forest, Agr. Forest Meteorol., 150, 389–398, 2010.

Inoue, Y., Penuelas, J., Miyata, A., and Mano, M.: Normalized difference spectral indices for estimating photosynthetic efficiency and capacity at a canopy scale derived from hyperspectral and CO_2 flux measurements in rice, Remote Sens. Environ., 112, 156–172, 2008.

Jin, H. and Eklundh, L.: A physically based vegetation index for improved monitoring of plant phenology, Remote Sens. Environ., 152, 512–525, doi:10.1016/j.rse.2014.07.010, 2014.

Kanniah, K. D., Beringer, J., Hutley, L. B., Tapper, N. J., and Zhu, X.: Evaluation of Collections 4 and 5 of the MODIS Gross Primary Productivity product and algorithm improvement at a tropical savanna site in northern Australia, Remote Sens. Environ., 113, 1808–1822, doi:10.1016/j.rse.2009.04.013, 2009.

Kanniah, K. D., Beringer, J., and Hutley, L. B.: The comparative role of key environmental factors in determining savanna productivity and carbon fluxes: A review, with special reference to Northern Australia, Prog. Phys. Geogr., 34, 459–490, 2010.

Kergoat, L., Lafont, S., Arneth, A., Le Dantec, V., and Saugier, B.: Nitrogen controls plant canopy light-use efficiency in temperate and boreal ecosystems, J. Geophys. Res., 113, 1–19, doi:10.1029/2007JG000676, 2008.

Leblanc, M. J., Favreau, G., Massuel, S., Tweed, S. O., Loireau, M., and Cappelaere, B.: Land clearance and hydrological change in the Sahel: SW Niger, Global Planet. Change, 61, 135–150, doi:10.1016/j.gloplacha.2007.08.011, 2008.

Levy, P. E., Moncrieff, J. B., Massheder, J. M., Jarvis, P. G., Scott, S. L., and Brouwer, J.: CO_2 fluxes at leaf and canopy scale in millet, fallow and tiger bush vegetation at the HAPEX-Sahel southern super-site, J. Hydrol., 188, 612–632, doi:10.1016/S0022-1694(96)03195-2, 1997.

Ma, X., Huete, A., Yu, Q., Restrepo-Coupe, N., Beringer, J., Hutley, L. B., Kanniah, K. D., Cleverly, J., and Eamus, D.: Parameterization of an ecosystem light-use-efficiency model for predicting

savanna GPP using MODIS EVI, Remote Sens. Environ., 154, 253–271, doi:10.1016/j.rse.2014.08.025, 2014.

Mayaux, P., Bartholomé, E., Massart, M., Cutsem, C. V., Cabral, A., Nonguierma, A., Diallo, O., Pretorius, C., Thompson, M., Cherlet, M., Pekel, J.-F., Defourny, P., Vasconcelos, M., Gregorio, A. D., Fritz, S., Grandi, G. D., Elvidge, C., Vogt, P., and Belward, A.: EUR 20665 EN, A Land-cover map of Africa, edited by: Centre, E. C. J. R., European Commisions Joint Research Centre, Luxembourg, 38 pp., 2003.

Mbow, C., Fensholt, R., Rasmussen, K., and Diop, D.: Can vegetation productivity be derived from greenness in a semi-arid environment? Evidence from ground-based measurements, J. Arid Environ., 97, 56–65, doi:10.1016/j.jaridenv.2013.05.011, 2013.

Merbold, L., Ardö, J., Arneth, A., Scholes, R. J., Nouvellon, Y., de Grandcourt, A., Archibald, S., Bonnefond, J. M., Boulain, N., Brueggemann, N., Bruemmer, C., Cappelaere, B., Ceschia, E., El-Khidir, H. A. M., El-Tahir, B. A., Falk, U., Lloyd, J., Kergoat, L., Le Dantec, V., Mougin, E., Muchinda, M., Mukelabai, M. M., Ramier, D., Roupsard, O., Timouk, F., Veenendaal, E. M., and Kutsch, W. L.: Precipitation as driver of carbon fluxes in 11 African ecosystems, Biogeosciences, 6, 1027–1041, doi:10.5194/bg-6-1027-2009, 2009.

Moncrieff, J. B., Monteny, B., Verhoef, A., Friborg, T., Elbers, J., Kabat, P., de Bruin, H., Soegaard, H., Jarvis, P. G., and Taupin, J. D.: Spatial and temporal variations in net carbon flux during HAPEX-Sahel, J. Hydrol., 188–189, 563–588, doi:10.1016/s0022-1694(96)03193-9, 1997.

Monteith, J. L.: Solar radiation and productivity in tropical ecosystems, J. Appl. Ecol., 9, 747–766, 1972.

Monteith, J. L.: Climate and the efficiency of crop production in Britain, Philos. T. Roy. Soc. B., 281, 277–294, 1977.

Monteny, B. A., Lhomme, J. P., Chehbouni, A., Troufleau, D., Amadou, M., Sicot, M., Verhoef, A., Galle, S., Said, F., and Lloyd, C. R.: The role of the Sahelian biosphere on the water and the CO_2 cycle during the HAPEX-Sahel experiment, J. Hydrol., 188, 516–535, doi:10.1016/S0022-1694(96)03191-5, 1997.

Mutanga, O. and Skidmore, A. K.: Narrow band vegetation indices overcome the saturation problem in biomass estimation, Int. J. Remote Sens., 25, 3999–4014, doi:10.1080/01431160310001654923, 2004.

NASA: Reverb ECHO: available at: http://reverb.echo.nasa.gov/reverb/, last access: 14 June 2016.

Papale, D., Reichstein, M., Aubinet, M., Canfora, E., Bernhofer, C., Kutsch, W., Longdoz, B., Rambal, S., Valentini, R., Vesala, T., and Yakir, D.: Towards a standardized processing of Net Ecosystem Exchange measured with eddy covariance technique: algorithms and uncertainty estimation, Biogeosciences, 3, 571–583, doi:10.5194/bg-3-571-2006, 2006.

Paruelo, J. M., Garbulsky, M. F., Guerschman, J. P., and Jobbágy, E. G.: Two decades of Normalized Difference Vegetation Index changes in South America: identifying the imprint of global change, Int. J. Remote Sens., 25, 2793–2806, doi:10.1080/01431160310001619526, 2004.

Poulter, B., Frank, D., Ciais, P., Myneni, R. B., Andela, N., Bi, J., Broquet, G., Canadell, J. G., Chevallier, F., Liu, Y. Y., Running, S. W., Sitch, S., and van der Werf, G. R.: Contribution of semi-arid ecosystems to interannual variability of the global carbon cycle, Nature, 509, 600–603, doi:10.1038/nature13376, 2014.

Prince, S. D., Kerr, Y. H., Goutorbe, J. P., Lebel, T., Tinga, A., Bessemoulin, P., Brouwer, J., Dolman, A. J., Engman, E. T., Gash, J. H. C., Hoepffner, M., Kabat, P., Monteny, B., Said, F., Sellers, P., and Wallace, J.: Geographical, biological and remote sensing aspects of the hydrologic atmospheric pilot experiment in the sahel (HAPEX-Sahel), Remote Sens. Environ., 51, 215–234, doi:10.1016/0034-4257(94)00076-Y, 1995.

Qi, J., Chehbouni, A., Huete, A. R., Kerr, Y. H., and Sorooshian, S.: A modified soil adjusted vegetation index, Remote Sens. Environ., 48, 119–126, 1994.

Richter, K., Atzberger, C., Hank, T. B., and Mauser, W.: Derivation of biophysical variables from Earth observation data: validation and statistical measures, J. Appl. Remote Sens., 6, 1–23, doi:10.1117/1.JRS.6.063557, 2012.

Rietkerk, M., Ketner, P., Stroosnijder, L., and Prins, H. H. T.: Sahelian rangeland development; a catastrophe?, J. Range Manage., 49, 512–519, 1996.

Rockström, J. and de Rouw, A.: Water, nutrients and slope position in on-farm pearl millet cultivation in the Sahel, Plant Soil, 195, 311–327, doi:10.1023/A:1004233303066, 1997.

Roujean, J.-L. and Breon, F.-M.: Estimating PAR absorbed by vegetation from bidirectional reflectance measurements, Remote Sens. Environ., 51, 375–384, doi:10.1016/0034-4257(94)00114-3, 1995.

Rouse, J. W., Haas, R. H., Schell, J. A., Deering, D. W., and Harlan, J. C.: Monitoring the Vernal Advancement of Retrogradation of Natural Vegetation, Type III, Final Report, Greenbelt, MD, 1974.

Ruimy, A., Saugier, B., and Dedieu, G.: Methodology for the estimation of terrestrial net primary production from remotely sensed data, J. Geophys. Res., 99, 5263–5283, 1994.

Running, S. W. and Zhao, M.: User's Guide, Daily GPP and Annual NPP (MOD17A2/A3) Products NASA Earth Observing System MODIS Land Algorithm, Version 3.0 For Collection 6., University of Montana, USA, NASA, 2015.

Running, S. W., Nemani, R. R., Heinsch, F. A., Zhao, M., Reeves, M., and Hashimoto, H.: A Continuous Satellite-Derived Measure of Global Terrestrial Primary Production, BioScience, 54, 547–560, doi:10.1641/0006-3568(2004)054[0547:ACSMOG]2.0.CO;2, 2004.

Scholes, R. J. and Archer, S. R.: Tree-grass interactions in savannas, Annu. Rev. Ecol. Syst., 28, 517–544, 1997.

Sellers, P. J., Dickinson, R. E., Randall, D. A., Betts, A. K., Hall, F. G., Berry, J. A., Collatz, G. J., Denning, A. S., Mooney, H. A., Nobre, C. A., Sato, N., Field, C. B., and Henderson-Sellers, A.: Modeling the Exchanges of Energy, Water, and Carbon Between Continents and the Atmosphere, Science, 275, 502–509, doi:10.1126/science.275.5299.502, 1997.

Sims, D. A., Rahman, A. F., Cordova, V. D., El-Masri, B. Z., Baldocchi, D. D., Flanagan, L. B., Goldstein, A. H., Hollinger, D. Y., Misson, L., Monson, R. K., Oechel, W. C., Schmid, H. P., Wofsy, S. C., and Xu, L.: On the use of MODIS EVI to assess gross primary productivity of North American ecosystems, J. Geophys. Res., 111, G04015, doi:10.1029/2006JG000162, 2006.

Sjöström, M., Ardö, J., Eklundh, L., El-Tahir, B. A., El-Khidir, H. A. M., Hellström, M., Pilesjö, P., and Seaquist, J.: Evaluation of satellite based indices for gross primary production estimates in a sparse savanna in the Sudan, Biogeosciences, 6, 129–138, 2009.

Sjöström, M., Zhao, M., Archibald, S., Arneth, A., Cappelaere, B., Falk, U., de Grandcourt, A., Hanan, N., Kergoat, L.,

Kutsch, W., Merbold, L., Mougin, E., Nickless, A., Nouvellon, Y., Scholes, R. J., Veenendaal, E. M., and Ardö, J.: Evaluation of MODIS gross primary productivity for Africa using eddy covariance data, Remote Sens. Environ., 131, 275–286, doi:10.1016/j.rse.2012.12.023, 2013.

Tagesson, T., Eklundh, L., and Lindroth, A.: Applicability of leaf area index products for boreal regions of Sweden, Int. J. Remote Sens., 30, 5619–5632, 2009.

Tagesson, T., Fensholt, R., Cropley, F., Guiro, I., Horion, S., Ehammer, A., and Ardö, J.: Dynamics in carbon exchange fluxes for a grazed semi-arid savanna ecosystem in West Africa, Agr. Ecosyst. Environ., 205, 15–24, doi:10.1016/j.agee.2015.02.017, 2015a.

Tagesson, T., Fensholt, R., Guiro, I., Rasmussen, M. O., Huber, S., Mbow, C., Garcia, M., Horion, S., Sandholt, I., Rasmussen, B. H., Göttsche, F. M., Ridler, M.-E., Olén, N., Olsen, J. L., Ehammer, A., Madsen, M., Olesen, F. S., and Ardö, J.: Ecosystem properties of semi-arid savanna grassland in West Africa and its relationship to environmental variability, Glob. Change Biol., 21, 250–264, doi:10.1111/gcb.12734, 2015b.

Tagesson, T., Fensholt, R., Huber, S., Horion, S., Guiro, I., Ehammer, A., and Ardö, J.: Deriving seasonal dynamics in ecosystem properties of semi-arid savanna grasslands from in situ-based hyperspectral reflectance, Biogeosciences, 12, 4621–4635, doi:10.5194/bg-12-4621-2015, 2015c.

Tagesson, T., Fensholt, R., Cappelaere, B., Mougin, E., Horion, S., Kergoat, L., Nieto, H., Ehammer, A., Demarty, J., and Ardö, J.: Spatiotemporal variability in carbon exchange fluxes across the Sahel, Agr. Forest Meteorol., 226–227, 108–118, 2016a.

Tagesson, T., Fensholt, R., Guiro, I., Cropley, F., Horion, S., Ehammer, A., and Ardö, J.: Very high carbon exchange fluxes for a grazed semi-arid savanna ecosystem in West Africa, Danish Journal of Geography, 116, 93–109, doi:10.1080/00167223.2016.1178072, 2016b.

Thenkabail, P. S., Smith, R. B., and De Pauw, E.: Hyperspectral Vegetation Indices and Their Relationships with Agricultural Crop Characteristics, Remote Sens. Environ., 71, 158–182, doi:10.1016/S0034-4257(99)00067-X, 2000.

Timouk, F., Kergoat, L., Mougin, E., Lloyd, C. R., Ceschia, E., Cohard, J. M., Rosnay, P. d., Hiernaux, P., Demarez, V., and Taylor, C. M.: Response of surface energy balance to water regime and vegetation development in a Sahelian landscape, J. Hydrol., 375, 12–12, doi:10.1016/j.jhydrol.2009.04.022, 2009.

Turner, D. P., Ritts, W. D., Cohen, W. B., Maeirsperger, T. K., Gower, S. T., Kirschbaum, A. A., Running, S. W., Zhao, M., Wofsy, S. C., Dunn, A. L., Law, B. E., Campbell, J. L., Oechel, W. C., Kwon, H. J., Meyers, T. P., Small, E. E., Kurc, S. A., and Gamon, J. A.: Site-level evaluation of satellite-based global terrestrial gross primary production and net primary production monitoring, Glob. Change Biol., 11, 666–684, 2005.

Turner, D. P., Ritts, W. D., and Cohen, W. B.: Evaluation of MODIS NPP and GPP products across multiple biomes, Remote Sens. Environ., 102, 282–293, 2006.

United Nations: Sahel Regional Strategy Mid-Year Review 2013, New York, 1–59, 2013.

Veenendaal, E. M., Kolle, O., and Lloyd, J.: Seasonal variation in energy fluxes and carbon dioxide exchange for a broadleaved semi-arid savanna (Mopane woodland) in Southern Africa, Glob. Change Biol., 10, 318–328, 2004.

Velluet, C., Demarty, J., Cappelaere, B., Braud, I., Issoufou, H. B.-A., Boulain, N., Ramier, D., Mainassara, I., Charvet, G., Boucher, M., Chazarin, J.-P., Oï, M., Yahou, H., Maidaji, B., Arpin-Pont, F., Benarrosh, N., Mahamane, A., Nazoumou, Y., Favreau, G., and Seghieri, J.: Building a field- and model-based climatology of local water and energy cycles in the cultivated Sahel – annual budgets and seasonality, Hydrol. Earth Syst. Sci., 18, 5001–5024, doi:10.5194/hess-18-5001-2014, 2014.

Yoder, B. J. and Pettigrew-Crosby, R. E.: Predicting nitrogen and chlorophyll content and concentrations from reflectance spectra (400–2500 nm) at leaf and canopy scales, Remote Sens. Environ., 53, 199–211, doi:10.1016/0034-4257(95)00135-N, 1995.

Zhang, Y., Guanter, L., Berry, J. A., Joiner, J., van der Tol, C., Huete, A., Gitelson, A., Voigt, M., and Köhler, P.: Estimation of vegetation photosynthetic capacity from space-based measurements of chlorophyll fluorescence for terrestrial biosphere models, Glob. Change Biol., 20, 3727–3742, doi:10.1111/gcb.12664, 2014.